

Model Analysis And Design Of Ellipse Based Segmented Varying Curved Foot For Biped Robot Walking

First Boyang Chen¹, Second Xizhe Zang¹, Third Chao Song^{1*},
Fourth Yue Zhang¹, Fifth Yan Liu¹, Sixth Jie Zhao¹

¹School of Mechatronics Engineering, Harbin Institute of Technology, 92 West Dazhi Street, Harbin, 150001, Heilongjiang, China.

*Corresponding author(s). E-mail(s): songchao@stu.hit.edu.cn;
Contributing authors: chenboyang@stu.hit.edu.cn;
zangxizhe@stu.hit.edu.cn; yzhanghit@stu.hit.edu.cn;
24B308015@stu.hit.edu.cn; jzhao@stu.hit.edu.cn;

Abstract

This paper presents the modeling, design, and experimental validation of an Ellipse-based Segmented Varying Curvature (ESVC) foot for bipedal robots. Inspired by the segmented curvature rollover shape of human feet, the ESVC foot aims to enhance gait energy efficiency while maintaining analytical tractability for foot location based controller. First, we derive a complete analytical contact model for the ESVC foot by formulating spatial transformations only using elementary functions. Then a nonlinear programming approach is engaged to determine the optimal elliptical parameters of hind and fore foot. Then an accuracy analysis is conducted for the single segment to address inaccuracies arising from model approximation, and an efficient piecewise compensation method is also provided. Finally, the proposed ESVC foot is integrated into a walking controller based on the Hybrid Linear Inverted Pendulum (HLIP) model, and validated through simulations and physical experiments on the TT II biped robot. Experimental results from marking time, sagittal walking, and lateral walking tasks demonstrate that the ESVC foot consistently reduces energy consumption compared to both line and flat feet, with particularly notable improvements during lateral walking. These findings suggest that the ESVC foot provides a practical and energy-efficient foot solution for legged robots.

Keywords: Biped Robot, Gait Energy efficiency, Varying Curvature Foot, Analytical Contact Model

1 Introduction

Legged robots, particularly in the quadruped and biped fields, have made significant progress recently, with a number of impressive movements now achievable. As the primary part interacting with the external environment, the robot foot not only participates in the evolution of the entire system dynamics, but also directly affects the gait energy efficiency, especially in control methods based on simplified models. Therefore, it is important to design a robot foot that achieves efficiency comparable to a biological foot[1–3].

To explore the effect of foot-ground contact on bipedal locomotion, researchers of human kinesiology and prosthetics have conducted a series of studies on biological structure, contact model and center of pressure trajectory[4–8]. They observed that the biological rollover shape can be segmented into three regions with varying curvature: fore-foot, mid-foot and hind-foot, and the fore-foot and hind-foot are more curved than mid-foot. This segmented varying curvature rollover shape enables high energy efficiency during human walking.

For legged-robot locomotion, the mainstream foot shapes can be categorized as arched foot[9][10], point foot[11, 12], flat foot[13], line foot[14], arc/curved foot[7, 11], biomimetic foot[15] and flexible heterogeneous foot[10]. To lower control complexity, researchers often prefer simplified foot designs. The simplest point foot has negligible mass, and the contact point can be considered fixed to the ground, which makes the kinematic and dynamic easy to analyze.[16, 17]. Therefore, it naturally benefits the model-based control methods such as Inverse Pendulum (IP). However, the point contact model can not provide sufficient frictional force/torque and is incapable to maintain static balance, especially especially when upper-body manipulation is involved. According to the research[7], the energy efficiency of point foot is also lower than the flatter types. Flat foot maintains a line contact in both sagittal and coronal plane and sufficient friction can be provided by the supporting polygon. Hence it is more widely used in humanoid robots such as Atlas[18] and Digit[19]. In contrast, using overly flat foot shape during walking means greater instantaneous impact and energy dissipation, making the gait less natural. Moreover, flat foot typically requires additional active degrees of freedom at ankle, which increase the foot weight and compromises mass centralization. Some robots transfer the actuators to the shank or waist via external linkages, such as Digit[19] and KUAVO[20], but the mechanism results more weight burden and requires futher motion space. Another widely used foottype is the line foot, which maintains the advantages of lightweight construction and structural simplicity, while also providing frictional torque to prevent self-rotation through line contact in the sagittal plane[14, 15, 21]. However, the constant flat line contact also results in limited energy efficiency. To enhance gait energy efficiency, arc/curved foot is often considered. The foot-ground contact point rollovers along the curved shape during support phase. Since it extends the contact duration, both the normal pressure and imact dissipation are reduced. Hence, the energy efficiency of arc/curved foot is superior to point foot and flat foot, besides, the biped robots with arc/curved foot exhibit a more human-like gait[7],[9],[22],[23],[24].

For the curved foot with constant curvature, it is not only unrealistic in biological foot, and the gait efficiency also differs significantly from that natural

shapes[6],[11],[15]. In other words, when extending the curved shape to three dimensions, it will resemble to a point foot. To pursue higher energy efficiency, researchers have incorporated the segmented variable curvature (SVC) feature from biological foot into robot foot design, and similar to biological counterpart, robot foot is also divided into three segments[7],[11],[24],[25],[26],[27]. Observation of the three parts of biological foot suggest that mid-foot is the flattest, while the forefoot and hind-foot are more curved. This shape characteristic is preserved in the bionic robot foot design to approximate the energy efficiency. Mahmoodi et al.[6] proposed a varying curved foot shape based on piecewise polynomial and confirmed that the segment curvature of the foot shape has a significant impact on gait period, walking speed, and inter-leg angles through bifurcation diagrams. Besides polynomial profiles, ellipse is also used to develop rollover shapes due to its natural varying curvature feature. Silva et al.[25] utilized two circle arcs and one flatten segment to form the rollover shape. Integrated with a 3D Linear Inverted Pendulum Model controller, the robot could reducing energy expenditure by almost 25% in simulation. However a completely flatten mid-foot neither meets the energy efficiency requirements nor the bionic features. Smyrli et al.[7] proposed a varying curvature foot using the single elliptical arc. Through numerical methods, the relationships between eccentricity, gait efficiency, stability, impact force and even walking speed are investigated. Their results indicate that for a targeted forward gait velocity, less pointy foot shapes, namely larger eccentricity for a certain minor axis, allow for higher gait energy efficiency. However, the analytical form of the contact model is not developed due to the incomplete elliptic integral. Besides the single-ellipse design can not allow the rollover shape been modified arbitrarily for application or bionic design as the curvature is coupled with the major and minor axes, and the evaluation is also nonphysical. In [27] and [28], researchers attempted to use a segmented convex rollover shape to simulate biological shape and derive its dynamic models. However, finding a suitable foot shape for robots is challenging, and thus, analytically represents the contact model remains difficult. For the arched foot, biomimetic foot, and flexible heterogeneous foot, which are designed for specific scenarios, are not within the discussion of this paper due to the specificity and complexity, as well as the difficulty in analyzing the contact effect on bipedal locomotion.

Considering the segmentary principle of biological foot, the varying curvature characteristics of elliptical arc and contact requirements of legged robot, the Ellipse-based Segmented Variable Curvature (ESVC) foot is proposed in this paper. Both the foot-ground contact model, design approach, and accuracy analysis of the ESVC Foot are discussed. The main contributions of this paper are as follows: first, we derive the space transformation for a single elliptical arc only based on elementary functions, then the contact model of entire ESVC foot model is given analytically. Second, a design approach of the ESVC foot is provided through nonlinear program, which uniquely determines the fore/hind segments. Third, an accuracy analysis is conducted to quantify the approximation error of space transformation and an efficient piecewise compensation method is also provided. Finally, the ESVC foot is integrated a model-based bipedal motion control framework and we evaluate the improvement of gait energy efficiency through physical experiments.

The organization of this paper is as follows: In Sec II.a, we introduce the assumptions and definitions of the key frames of the ESVC Foot. In Sec II.b, the spatial transformation for single elliptical arc is derived. Then we provide the design approach (Sec II.c) and the entire analytical contact model of ESVC foot (Sec II.d). In Sec II.e, anaccuracy analysis and compensation is investigated. The integration of the ESVC Foot and model-based control is described in Sec III. In Sec IV, physical walking experiments is conducted to evaluate the proposed foot. Conclusion and future work are presented in Sec V.

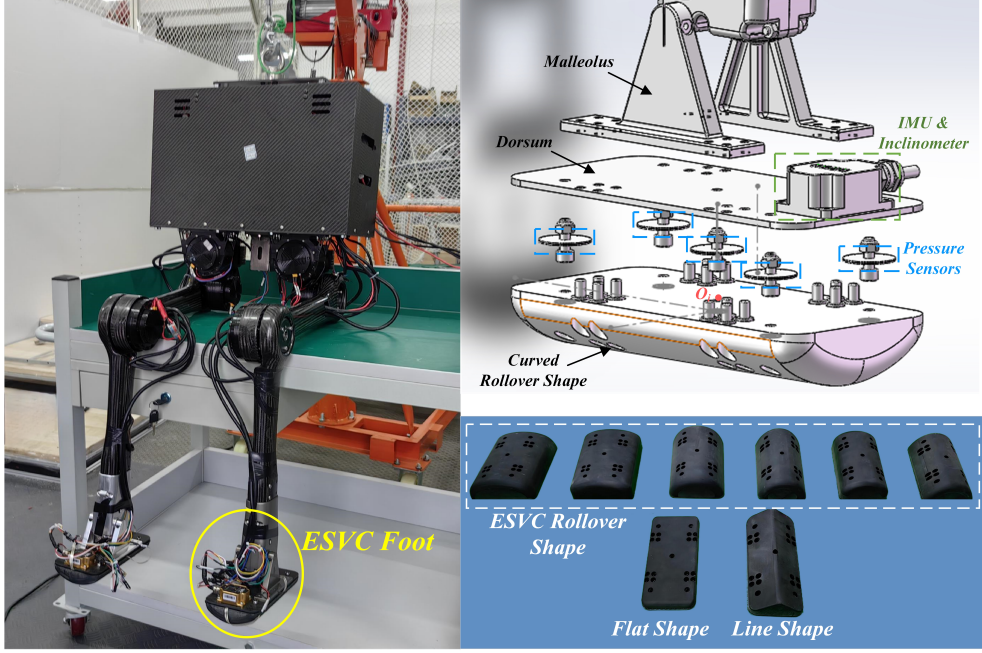


Fig. 1 a.Biped Robot TT II With ESVC Foot; b.The Assembly Drawing Of ESVC Foot; c.Rollover Shape Of Different Foot Types

2 Geometric Analysis and Contact Model of ESVC Foot

2.1 Preliminary

2.1.1 Foot Shape Specification

Directly replicating biological data for robotic foot design is inappropriate not only because the evolution of robot systems differ fundamentally from human, but also because robotic feet must be analytically tractable. Considering practical applications, the proposed ESVC foot is designed like a flat-bottom boat, as shown in Fig1. In the

sagittal plane, the ESVC foot establishes a line contact similar to that of a flat foot which aims to provide frictional torque from self-rotation. In the coronal plane, three elliptical arcs are engaged to approximate the segmented varying curvature features of biological rollover shape. For consistency in terminology, the segments still named by: *hind*, *mid* and *fore*. That is to say the eccentricity of mid ellipse is larger than hind/fore ellipse, and hind ellipse and fore ellipse are symmetric w.r.t. the mid line of ESVC foot.

2.1.2 Assumptions & Key Frames Define

Sample body text. Sample body text.

2.1.3 Assumptions & Key Frames Define

Before analyzing the spacial transformation of ESVC foot, some assumptions need to be introduced:

F1: The contact of foot-ground is assumed to be rigid and the foot will not deform;

F2: The foot roll on the ground without slipping during the support phase. When the assumptions are satisfied, the contact point will rollover along the sole surface. Hence, the state of the center of mass (COM) and the swing foot w.r.t. contact point is time variant.

To analyze this time-varying model, we divide the entire robotic system into internal space and external space by a fixed frame which is located at the center of foot upper surface and called *foot frame*. In the internal space, the states of CoM and the swing foot only depend on the joint states, which is easy to calculate. In external space, the transition between the foot frame and contact point frame is important that once the spacial transformation can be expressed analytically, the state of CoM and the pre-contact point of the swing foot are determined. For more complex tasks, such as climbing stairs, precise foot placement planning is essential. Therefore, the transition between the world frame and the contact frame, specifically the rollover length, must be determined. For simplicity, we use a fixed contact frame with 0 roll angle replace the world frame. At this point, the three key frames of the ESVC foot can be defined: foot frame O_i , fixed frame O_c , and contact frame C , as shown in Fig2.

2.2 Model Analysis of Single Elliptic Arc

The overall rollover process of contact point on the ESVC foot is described in Fig2. Fig2.a shows the case when the foot rollover angle is 0, where the contact point locates at the origin of fixed frame O_c . Fig2.b and Fig2.c depict the contact point rolls within the mid ellipse and the hind/fore ellipse. Fig2.d represents the case just before the foot lifts off the ground which can be considered the toe is to leave the ground.

For single elliptical arc, the transformation matrices between the three key frames depend on the rollover length and the rollover angle of ellipse. The rollover angle of ellipse is defined as the angle between the line connecting the contact point and the foot frame origin, and the minor axis, namely ϕ_m . When foot tilts from left to right and the rollover range within the mid ellipse(Fig2.b), the minor axis coincides with

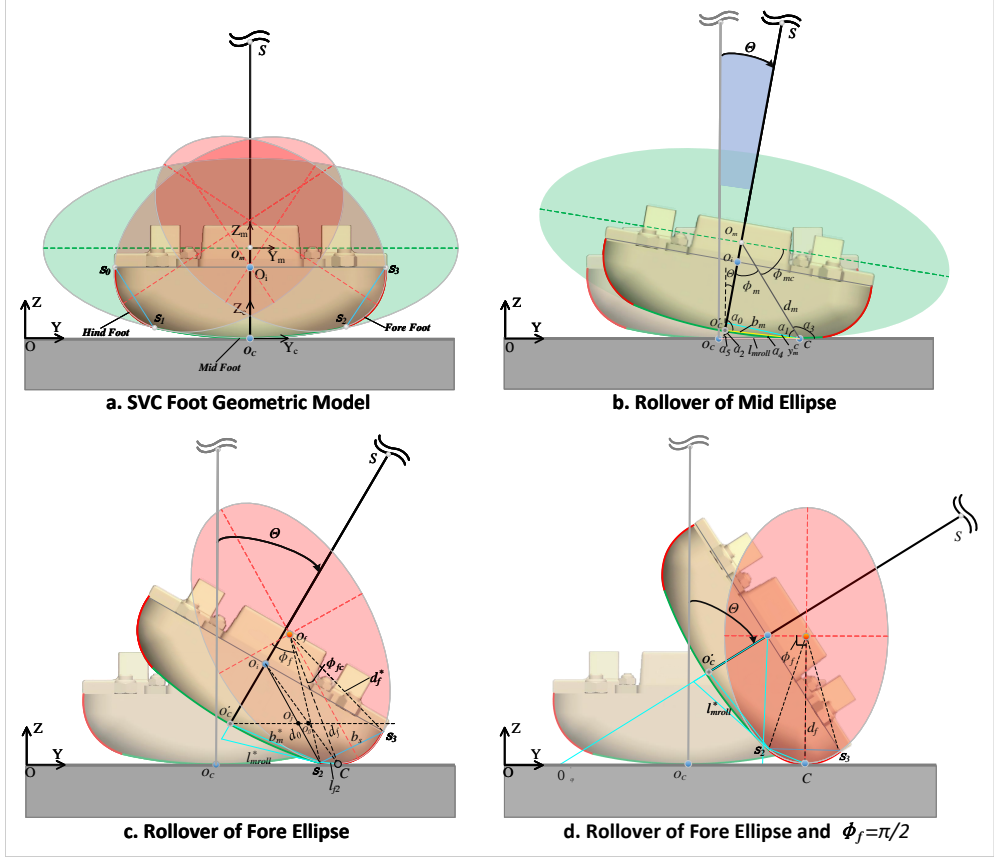


Fig. 2 Rollover Process of ESVC Foot

the vertical axis of the foot frame. The roll angle of foot θ is defined between the foot frame and the world frame which can be obtained from inclinometer. Assuming $\theta_m = |\theta|$, then the rollover angle of mid ellipse ϕ_m and its complementary angle ϕ_{mc} can be calculated:

$$\begin{cases} \phi_{mc} = \tan^{-1}\left(\frac{r_{mb}^2}{r_{ma}^2 \tan \theta_m}\right) \\ \phi_m = \frac{\pi}{2} - \phi_{mc} \end{cases} \quad (1)$$

Then the distance and Y-coordinate of the contact point C to w.r.t. the mid ellipse center frame can be expressed as:

$$\begin{cases} d_m = \left(\frac{r_{ma}^2 r_{mb}^2}{r_{ma}^2 \cos^2 \phi_m + r_{mb}^2 \sin^2 \phi_m} \right)^{\frac{1}{2}} \\ y_C^m = d_m \sin \phi_m \end{cases} \quad (2)$$

The elliptical parameter angle is:

$$\lambda_m = \sin^{-1} \frac{y_C^m}{r_{ma}} \quad (3)$$

The rollover length of contact point C , namely the ellipse arc length of ϕ_m is define through the incomplete elliptic integral:

$$l_{mroll} = r_{ma} \int_0^\lambda \sqrt{1 - e_m^2 \sin^2 \lambda_m} d\lambda_m \quad (4)$$

Unfortunately, this integral cannot be calculated directly, hence an approximation from [29] utilizing elementary functions is egaged:

$$l_{mrolla} = r_{ma} (\lambda_m - (\lambda_m - \sin \lambda_m) \frac{2k_m}{\pi} - \xi (\pi - (\pi - 2) \frac{2k_m}{\pi} - 2E_m) \frac{\lambda_m - \lambda_m^*}{\pi - 2\lambda_m^*}) \quad (5)$$

Let e_m be the eccentricity of the mid ellipse, then the modulus angle is $k_m = \sin^{-1} e_m$. Parameter E_m depend on k_m , and ξ is binary variable relative to λ_m^* :

$$\begin{cases} E_m = \frac{\pi r_{mb} + 4(r_{ma} - r_{mb})}{4r_{ma}} \left(1 + \left(\frac{r_{mb}}{r_{ma}} \right)^{\frac{3}{2}} \right) \\ \lambda_m^* = \frac{36k_m + 13\pi}{52} \end{cases} \quad (6)$$

$$\xi = \begin{cases} 0, & \lambda_m < \lambda_m^* \\ 1, & \lambda_m \geq \lambda_m^* \end{cases} \quad (7)$$

Since both the fixed frame O_C and the contact frame C are aligned to the world frame, the transformation between two frames can be derived analytically:

$${}_{O_C}^C T_m = \begin{bmatrix} 1 & 0 & 0 & 0 \\ 0 & 1 & 0 & sgn(\theta) l_{mrolla} \\ 0 & 0 & 1 & 0 \\ 0 & 0 & 0 & 1 \end{bmatrix} \quad (8)$$

For the transformation of contact frame and the foot frame, the matrix can be solved through the frame O'_C . The inside chord length b_m , as depicted by the yellow dashed line in Fig2.b, is determined by:

$$b_m = (d_m^2 + r_{mb}^2 - 2d_m r_{mb} \cos \phi_m)^{\frac{1}{2}} \quad (9)$$

Then the auxiliary angles($\alpha_0 \sim \alpha_5$) is:

$$\begin{cases} \alpha_0 = \sin^{-1} \left(\frac{d_m \sin \phi_m}{b_m} \right) \\ \alpha_1 = \sin^{-1} \left(\frac{r_{mb} \sin \phi_m}{b_m} \right) \\ \alpha_2 = \pi - \alpha_0 \\ \alpha_3 = \pi - \phi_{mc} - \theta_m \\ \alpha_4 = \pi - \alpha_3 - \alpha_1 \\ \alpha_5 = \pi - \alpha_2 - \alpha_4 \end{cases} \quad (10)$$

The Y-coordinate and Z-coordinate of O'_C in frame C can be represented:

$$\begin{cases} y_{O'_C}^C = \text{sgn}(\theta) b_m \cos \alpha_4 \\ z_{O'_C}^C = b_m \sin \alpha_4 \end{cases} \quad (11)$$

Then the transformation of frame O'_C to frame C is:

$${}_{O'_C}^C T_m = \begin{bmatrix} 1 & 0 & 0 & 0 \\ 0 & \cos \theta_m & \sin \theta_m & y_{O'_C}^C \\ 0 & -\sin \theta_m & \cos \theta_m & z_{O'_C}^C \\ 0 & 0 & 0 & 1 \end{bmatrix} \quad (12)$$

As the transformation of frame O_i and frame O'_C is constant:

$${}_{O'_C}^{O_i} T_m = \begin{bmatrix} 1 & 0 & 0 & 0 \\ 0 & 1 & 0 & 0 \\ 0 & 0 & 1 & h_{foot} \\ 0 & 0 & 0 & 1 \end{bmatrix} \quad (13)$$

The matrix of frame O_i and frame C can be easily obtained:

$${}_{O_i}^C T_m = {}_{O'_C}^C T_m * {}_{O'_C}^{O_i} T_m \quad (14)$$

Now the transformation of the three key frames of ESVC foot is derived analytically.

2.3 Rollover Shape Design of Hind Foot and Fore Foot

Before we derive the model of hind/fore foot, the rollover shape should be determined. Although the profiles of rollover shape has been selected, determining the parameters remains a challenging task. There are two key questions: how the curvature varies, and where the segmentation points are located. Unfortunately it is difficult to answer them currently. From a designer perspective, the various attributes of the robot, such

as nature dynamics, target gaits, and even optimization objectives, can lead to various optimal rollover shapes. From the perspective of gait efficiency, establishing an accurate contact model is a prerequisite for linking gait performance with design parameters. Fortunately, some conclusions regarding single elliptical arc foot are provided in [7]. Therefore, our idea is that if we can find all the parameters of ESVC foot based on partial parameters. In other words, assuming the mid ellipse is known in advance, we need a method to determine the hind/fore ellipse uniquely.

Without compromising flexibility, we introduce two assumptions:

F3: At the segment points S_2 and S_3 , the tangent slope of the mid ellipse should be as consistent as possible with the hind/fore ellipse;

F4: The perpendicular bisector of S_2S_3 coincides with the major axis of the fore ellipses.

Superscript * is used to denote the situation when the contact point locates at segment point. Taking fore ellipse as the example, then the rollover angle of mid ellipse is denoted by ϕ_m^* , with corresponding parameters b_m^* , ϕ_{mc}^* , l_{mrolla}^* , $\alpha_0^* \sim \alpha_5^*$ and θ_m^* . In $\triangle O_iO'_CS_2$, the distance of O_iS_2 and the angle to the minor axis of mid ellipse is:

$$\begin{cases} d_0 = \left(h_{foot}^2 + b_m^{*2} - 2h_{foot}b_m^* \cos \alpha_0^* \right)^{\frac{1}{2}} \\ \alpha_6 = \sin^{-1} \frac{b_m^* \sin \alpha_0^*}{d_0} \end{cases} \quad (15)$$

Then the $\triangle O_iS_2S_3$ can be solved as:

$$\begin{cases} \alpha_7 = \frac{\pi}{2} - \alpha_6 \\ b_s = \left(\frac{w_{foot}^2}{4} + d_0^2 - w_{foot}d_0 \cos \alpha_7 \right)^{\frac{1}{2}} \\ \alpha_8 = \sin^{-1} \frac{d_0 \sin \alpha_7}{b_s} \end{cases} \quad (16)$$

For the fore ellipse, there are four unknown parameters including major and minor axis r_{fa} and r_{fb} , rollover angle ϕ_f^* and d_f^* , the distance of O_fS_2 . From F4, the distance of S_2S_3 satisfies:

$$\frac{b_s}{2} = \sin \left(\frac{\pi}{2} - \phi_f^* \right) d_f^* \quad (17)$$

where d_f^* can be obtain using Eq.2. As $\alpha_8 = \alpha_{10}$, then θ_f^* and θ_m^* satisfies Eq.18, where the relationship of ϕ_f^* and θ_f^* is similar to Eq.1.

$$\theta_f^* - \theta_m^* = \frac{\pi}{2} - \sin^{-1} \frac{d_0 \sin \alpha_7}{b_s} \quad (18)$$

If the constraint that the slopes of the two ellipses are equal at the segmentation point is enforced, there are four equations for the four parameters. Due to the nonlinearity, the equations may not have a solution. Hence, we relax the constraint as F3.

The slope at S_2 of the two ellipse can be calculated as:

$$\begin{cases} \eta_m^* = \frac{r_{mb}^2}{r_{ma}^2} \tan \phi_m^* \\ \eta_f^* = \frac{r_{fb}^2 \tan \phi_f^* - r_{fa}^2 \tan \theta_f^*}{r_{fa}^2 + r_{fb}^2 \tan \theta_f^* \tan \phi_f^*} \end{cases} \quad (19)$$

Then four parameters can be solved using a nonlinear program:

$$\begin{aligned} & \min_{\mathbf{r}_{fa}, \mathbf{r}_{fb}, \phi_f^*, \mathbf{d}_f^*, \mathbf{w}_{foot}, \theta_f^*} && w_1(\eta_m^* - \eta_f^*)^2 + w_2 r_{fa}^2 + w_3 r_{fb}^2 + w_4(w_{foot} - w_{foot}^*)^2 \\ & \text{s.t.} && \text{Eq.17, Eq.18;} \\ & && \cot \phi_f^* = \frac{r_{fb}^2}{r_{fa}^2 \tan \theta_f^*}; \\ & && d_f^* = \left(\frac{r_{fa}^2 r_{fb}^2}{r_{fa}^2 \cos^2 \phi_f^* + r_{fb}^2 \sin^2 \phi_f^*} \right)^{\frac{1}{2}}; \\ & && \frac{w_{foot}}{2} \geq d_0 \sin \alpha_6; \\ & && \eta_f^{*2} \geq \eta_m^{*2}; \\ & && e_m \geq e_f; \\ & && r_{fa} \geq r_{fb}; \\ & && r_{fa}, r_{fb}, \phi_f^*, d_f^* \geq 0. \end{aligned} \quad (20)$$

The decision variables include foot width w_{foot} , θ_f^* and the four design parameters. w_1 , w_2 , w_3 and w_4 are the weight of cost function. Boundary constraints that $\phi_f^* \in (0, \frac{\pi}{2})$, $d_f^* \in (0, 0.5)$ and $w_{foot} \in (0, 0.2)$ should be incorporated. By adjusting the w_1 , the smoothness of the segment point can be controlled. It is worth noting that we do not specify the foot width in advance, and through w_4 , and nominal foot width w_{foot}^* , w_{foot} can also be found.

Once the mid ellipse is known, the fore/hind ellipse can be uniquely determined. This does not mean that we lose the design flexibility. As we do not enforce the location of segment point S_2 , hind/mid/fore ellipse can be adjusted arbitrarily. In other words, ϕ_m^* becomes a freedom of the design approach. Therefore, the ESVC foot can mimic any biological foot and the deficiency of single ellipse foot is compensated.

2.4 Model Analysis of Fore/Hind Foot

Now, we continually derived the contact model of fore foot. Theoretically, the roll angle of ESVC foot $\theta \in (0, \frac{\pi}{2})$, and according to Eq.18, θ_f and ϕ_f may large than $\frac{\pi}{2}$. Hence,

ϕ_f can be separated as:

$$\phi_f = \begin{cases} \frac{\pi}{2} - \tan^{-1} \frac{r_{fb}^2}{r_{fa}^2 \tan \theta_f}, & \theta_f \in \left(\theta_m^* + \frac{\pi}{2} - \alpha_{10}, \frac{\pi}{2} \right) \\ \frac{\pi}{2} + \tan^{-1} \frac{-r_{fb}^2}{r_{fa}^2 \tan \theta_f}, & \theta_f \in \left(\frac{\pi}{2}, \pi - \alpha_{10} \right) \end{cases} \quad (21)$$

As $\phi_f \in \left(\phi_f^*, \frac{\pi}{2} \right]$, the arc length of S_2C can be calculated as:

$$l_{froll} \approx l_{frolla} = l_{f\phi_f} - l_{f\phi_f}^* \quad (22)$$

$l_{f\phi_f}$ and $l_{f\phi_f}^*$ are the rollover length of ϕ_f and ϕ_f^* , respectively, and the value can be calculated as Eq.5. Then the transformation of the fixed frame and the contact frame of the fore ellipse is:

$${}^C_O T_f = \begin{bmatrix} 1 & 0 & 0 & 0 \\ 0 & 1 & 0 & sgn(\theta)(l_{mrolla} + l_{frolla}) \\ 0 & 0 & 1 & 0 \\ 0 & 0 & 0 & 1 \end{bmatrix} \quad (23)$$

To determine the transformation of the foot frame and the contact frame of fore ellipse, we need to derive the length of O_iC and its angle to the horizontal axis. In $\triangle O_f S_2 C$, $\angle S_2 O_f C$ and the length of $O_f C$ are:

$$\begin{cases} \alpha_9 = \phi_f - \phi_f^* \\ d_f = \left(\frac{r_{fa}^2 r_{fb}^2}{r_{fa}^2 \cos^2 \phi_f + r_{fb}^2 \sin^2 \phi_f} \right)^{\frac{1}{2}} \end{cases} \quad (24)$$

Then the chord length of S_2C and $\angle O_f S_2 C$ are:

$$\begin{cases} b_f = \left(d_f^{*2} + d_f^2 - 2d_f^* d_f \cos \alpha_9 \right)^{\frac{1}{2}} \\ \alpha_{11} = \sin^{-1} \frac{d_f \sin \alpha_9}{b_f} \end{cases} \quad (25)$$

In $\triangle O_i S_2 S_3$, $\angle O_i S_2 S_3$ is :

$$\alpha_{12} = \pi - \alpha_8 - \alpha_7; \quad (26)$$

Then $\angle O_i S_2 O_f$ and $\angle O_i S_2 C$ can be calculated by assumption F4:

$$\begin{cases} \alpha_{13} = \alpha_{12} - \phi_f^* \\ \alpha_{14} = \alpha_{13} + \alpha_{11} \end{cases} \quad (27)$$

Hence, the length of O_iC in $\triangle O_iS_2C$ is:

$$l_{fO_iC} = (b_f^2 + d_0^2 - 2b_f d_0 \cos \alpha_{14})^{\frac{1}{2}} \quad (28)$$

In $\triangle O_iS_2C$, $\angle S_2O_iC$ satisfies:

$$\alpha_{15} = \sin^{-1} \frac{b_f \sin \alpha_{14}}{l_{fO_iC}} \quad (29)$$

The auxiliary angle α_{16} which are defined as the angle between S_2O_i and the horizontal axis and its complementary angle α_{17} can be calculated:

$$\begin{cases} \alpha_{16} = \frac{\pi}{2} - \alpha_6 + \theta_m \\ \alpha_{17} = \frac{\pi}{2} + \alpha_6 - \theta_m \end{cases} \quad (30)$$

Then, the angle between O_iC and the horizontal axis is:

$$\alpha_{18} = \frac{\pi}{2} - \alpha_6 + \theta_m - \alpha_{15} \quad (31)$$

Finally, the transformation of the foot frame and the contact frame C as $\phi_f \in (\phi_f^*, \frac{\pi}{2}]$ is:

$${}^C_O T_f = \begin{bmatrix} 1 & 0 & 0 & 0 \\ 0 & \cos \theta_m & \sin \theta_m & sgn(\theta) l_{fO_iC} \cos \alpha_{18} \\ 0 & -\sin \theta_m & \cos \theta_m & l_{fO_iC} \sin \alpha_{18} \\ 0 & 0 & 0 & 1 \end{bmatrix} \quad (32)$$

When $\phi_f \in (\frac{\pi}{2}, \pi - \phi_f^*]$, the transition of the key frames can be derived similarly and will not discuss here. However, if $\theta \rightarrow \frac{\pi}{2}$, the com axis becomes parallel to the ground which means the robot will fall. Therefore, $\theta_f = \frac{\pi}{2}$ can be defined as the toe edge of the ESVC foot.

2.5 Accuracy Analysis of ESVC Foot Model

Before integrating the ESVC foot with the bipedal robot, we need to address a remained question. In the contact model, ${}^C_O T_m$ and ${}^C_O T_f$ are the analytical form, but the rollover length calculated by Eq.5 and Eq.22 is an approximating result. In this section, we will analyse the error and provide a compensation method.

For intuitive understanding, we selected three elliptical arcs with different eccentricities as the comparison subjects and the rollover angle varies from 0 to $\frac{\pi}{2}$. The major and minor axis of Ellipse Arc(EA)1 is [0.04575, 0.03750]. These values are derived from [7], a combination of high stability with relatively small values. The major and minor axis of EA2 and EA3 are [0.05205, 0.03150] and [0.06901, 0.02595], respectively. EA1 is closer to a circle, while EA2 lies between EA3 and EA1. More importantly, the boundary parameter angle λ^* of EA3 is equal to 1.606 which is larger than $\frac{\pi}{2}$ and

the switching parameter ξ is always 0. The value of λ^* of EA1 and EA2 are 1.2077 and 1.4229, respectively, which indicates that the ξ can be triggered. Nevertheless, as the λ^* of EA2 is relatively large, which reduces the possibility of triggering during the rollover process. In contrast, the boundary parameter angle of EA1 is relatively small, making it more likely to be triggered. Therefore, EA1, EA2 and EA3 represents the three typical ESVC foot for error analysis.

The ground truth are obtained by the numerical method of Eq.4 and the accuracy is quantified by error percentage:

$$P_{Err} = \frac{l_{rolla} - l_{roll}}{l_{roll}} \times 100\% \quad (33)$$

The result of EA1, EA2 and EA3 are shown in Fig3, where different line styles represent different arcs, and color represent different approximation, that black is the inner chord approximation, blue is the approximation of Eq.5. From the comparison, it can be observed that both maximum error and average error of Eq.5 are much smaller than the inside the chord. However, it is still too large for modeling contact and robot control due to the amplification effect of the supporting leg. We also found that the error shapes of Eq.5 are all sine-like waveform. Therefore a compensation method can be proposed based on the error shape:

$$\tilde{l}_{rolla} = \begin{cases} l_{rolla} - sgn(\delta_{max})K_e\delta_{max} \sin\left(\frac{\lambda - 2\lambda^* + \frac{\pi}{2}}{\pi - 2\lambda^*}\right), & \lambda^* < \frac{\pi}{2} \\ l_{rolla} - sgn(\delta_{max})K_e\delta_{max} \sin\left(\frac{\theta - 2\theta_{\delta_{max}} + \frac{\pi}{2}}{\pi - 2\theta_{\delta_{max}}}\right), & \lambda^* \geq \frac{\pi}{2} \end{cases} \quad (34)$$

δ_{max} is the maximum error of $[0, \frac{\pi}{2}]$. K_e is the gain for compensation. $\theta_{\delta_{max}}$ is the roll angle of maximum error when $\lambda^* \geq \frac{\pi}{2}$. The compensated result is depicted as the green lines in Fig3.

The accurate performacne of average error and max error is given in Table1, where it is obvious that the accuracy improvement of the proposed compensation method(Eq.34) is significant. For instance, considering the EA3 that used for the mid-foot, the average error of the compensation method is only 14.04% to Eq.5 and the maximum error is 27.78%. Compared to the inner chord approximation, Eq.34 has achieved an improvement of over ten times, both in terms of maximum error and average error. Additionally, in terms of value magnitude, the compensation method is very close to the ground truth, which will efficiently benefit the calculation of differential velocity.

3 Integration of ESVC Foot And Model-Based Control

In this section we will demonstrate how to integrated the ESVC foot with the model-based control.

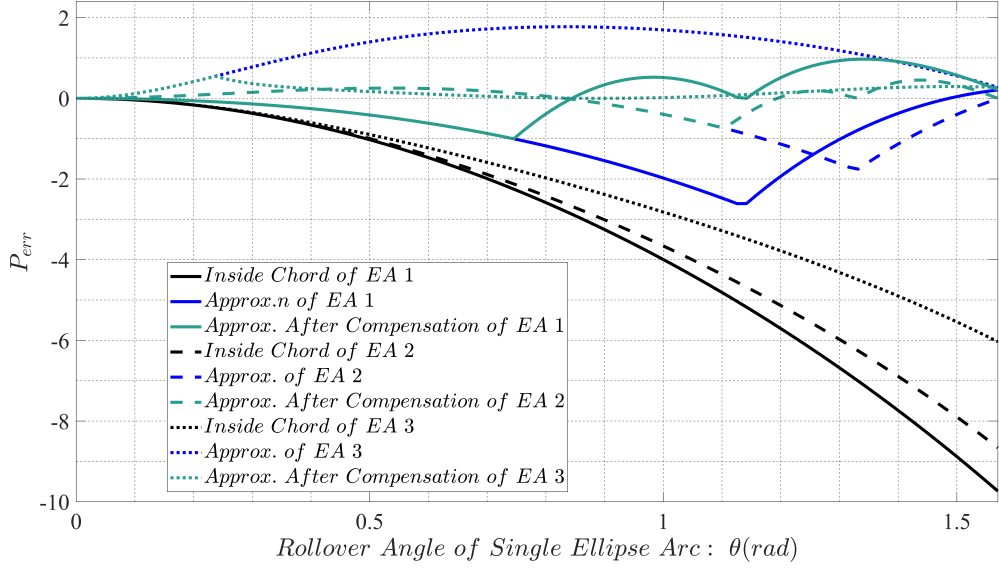


Fig. 3 Accuracy Of Rollover Length For Different Ellitical Arcs

Table 1 Accuracy Performance of Different Elliptical Arc

/	EA1 Chord9	EA1 (Eq.5)	EA1 (Eq.34)	EA2 Chord9	EA2 (Eq.5)	EA2 (Eq.34)	EA3 Chord9	EA3 (Eq.5)	EA3 (Eq.34)
λ^*	1.2077	1.2077	1.2077	1.4229	1.4229	1.4229	1.6062	1.6062	1.6062
Max δ	-9.73%	-2.61	+0.97%	-8.68%	-1.57%	-0.68%	-6.04%	+1.77%	+0.49%
Avr δ	-3.29%	-0.81	-0.07%	-2.99%	-0.28%	-0.05%	-2.25%	+1.14%	+0.16%

3.1 Kinematic Model of Biped Robot with ESVC Foot

Using Eq.35 updates the approximation of rollover length l_{rolla} according to Eq.5 and Eq.22:

$$\tilde{l}_{rolla} = \begin{cases} \tilde{l}_{mrolla}, & \theta \in [0, \theta_m^*) \\ \tilde{l}_{mrolla} + \tilde{l}_{frolla}, & \theta \in [\theta_m^*, \alpha_{10}) \\ \tilde{l}_{mrolla} + \tilde{l}_{f\frac{\pi}{2}} - \tilde{l}_{f\phi'_f}, & \theta \in [\alpha_{10}, \frac{\pi}{2}) \end{cases} \quad (35)$$

The transformation of the foot frame and the contact frame of roll rotation can be obtained from Eq.14 and Eq.32. Here we collectively refer to ${}^C_{O_i}T_m$ and ${}^C_{O_i}T_f$ as ${}^C_{O_i}T$. The superscript r denotes the roll rotation. As foot does not deform, when the pitch angle β is nonzero, the new contact point is located at the edge in X direction and

the transformation matrix is denoted as ${}_{O_i}^{Cp}T$:

$${}_{O_i}^{Cp}T = \begin{bmatrix} \cos \beta & 0 & \sin \beta & -\frac{l_{foot}}{2} \cos \beta \\ 0 & 1 & 0 & 0 \\ -\sin \beta & 0 & \cos \beta & \frac{l_{foot}}{2} \cos \beta \\ 0 & 0 & 0 & 1 \end{bmatrix} \quad (36)$$

For yaw rotation, the transformation ${}_{O_i}^{Cy}T$ is easy to write:

$${}_{O_i}^{Cy}T = \begin{bmatrix} \cos \gamma & -\sin \gamma & 0 & 0 \\ \sin \gamma & \cos \gamma & 0 & 0 \\ 0 & 0 & 1 & 0 \\ 0 & 0 & 0 & 1 \end{bmatrix} \quad (37)$$

Then the entire transformation of the foot frame and the contact frame is:

$${}_{O_i}^CT_{ESVC} = {}_{O_i}^{Cy}T * {}_{O_i}^{Cp}T * {}_{O_i}^{Cr}T \quad (38)$$

Similarly, the transition of the fixed frame and the contact frame is

$${}_{O_C}^CT_{ESVC} = {}_{O_C}^{Cy}T * {}_{O_C}^{Cp}T * {}_{O_C}^{Cr}T \quad (39)$$

Then the position of COM and the pre-contact of swing foot respect to contact frame is obtained:

$$\begin{cases} p_{com}^C(t) = {}_{O_i}^CT_{ESVC} \begin{bmatrix} f(q_i(t)) \\ 1 \end{bmatrix} \\ p_{sw}^C(t) = {}_{O_i}^CT_{ESVC} \begin{bmatrix} g(q_i(t), \theta_{sw}) \\ 1 \end{bmatrix} \end{cases} \quad (40)$$

$f(\cdot)$ represents the com position w.r.t. the foot frame which only depend on joint position and $g(\cdot)$ calculates the pre-contact point of swing foot. θ_{sw} is the roll angle of swing foot which is used to conduct the same calculation for the pre-contact point w.r.t. the swing foot frame. ${}_{O_i}^CT_{sp}$ is the transformation of the foot frame and the contact frame of support foot. For the coordinates with respect to the absolute frame, it is also easy to obtain through the transformations of the key frames:

$$\begin{cases} p_{com}^{O_C}(t) = {}_{O_C}^CT_{ESVC}^{-1} * {}_{O_i}^CT_{ESVC} \begin{bmatrix} f(q_i(t)) \\ 1 \end{bmatrix} \\ p_{sw}^{O_C}(t) = {}_{O_C}^CT_{ESVC}^{-1} * {}_{O_i}^CT_{ESVC} \begin{bmatrix} g(q_i(t), \theta_{sw}) \\ 1 \end{bmatrix} \end{cases} \quad (41)$$

3.2 HLIP Control with ESVC Foot

Hybrid Linear Inverted Pendulum(HLIP)[30] is an outstanding model-based control method with two phases: single support phase(SSP) and double support phase(DSP),

that exhibiting excellent performance on Cassie. For simplicity, we set the duration of DSP to zero in this paper.

HLIP occupies a linear Step to Step(S2S) dynamics that the target step length is determined by the desired step length, the desired HLIP state and the robot pre-impact state:

$$\begin{cases} X_k^R = AX_{k-1}^R + Bu_{k-1}^R \\ u_k^R = u_k^h + K(X_k^R - X_k^h) \end{cases} \quad (42)$$

X_{k-1}^R is the impact state of the robot relative to the support location for current step and u_{k-1}^R is the executed step length. A and B are the state transformation matrix and input matrix. X_k^h and u_k^h are the desired HLIP state and desired step length derived from stabilization of S2S dynamics, respectively. u_k^R the is the target step length of the robot stabilization.

To verify the effectiveness of the ESVC foot, the robot is required to behave in accordance with the HLIP constraints. The gait generation and feedback control carried out w.r.t. the contact frame. Taking single step as instance, the feedback pre-impact state of COM X_{fdcom}^C can be calculated as:

$$[p_{fdcom}^C \ 1 \ v_{fdcom}^C \ 1]^T = \begin{bmatrix} {}_O^C T_{sp} & 0 \\ {}_O^C T_{sp} & {}_O^C T_{sp} \end{bmatrix} [p_{fdcom}^{O_i} \ 1 \ v_{fdcom}^{O_i} \ 1]^T \quad (43)$$

$\dot{{}_O^C T}_{sp}$ is the first order derivative of ${}_O^C T_{sp}$. Although the transformation is composed of elementary functions, the derivative is too long to program. In practical applications, numerical methods is often engaged to obtain it. Substituting X_{fdcom}^C into Eq.42, the target step length with ESVC foot is obtained. The state swing foot pre-contact point $X_{fdsw}^C(t)$ can be achieved similarly. Then the swing foot of robot is stabilized by Eq.44 and K_{swa} is the correct gain. Joint level controller is identical that in [30].

$$x_{swC}^d(t) = x_{swC}^*(t) + K_{swa}(X_{fdsw}^C(t) - x_{swC}^*(t)) \quad (44)$$

4 Implementation and Experiment

To validate the proposed ESVC Foot, we implement three ESVC feet as described in Sec2.5 and compare with line foot and flat foot through physical experiments. The foot prototypes with TT II robot is shown in Fig1.

4.1 Simulation

To verify stability, straight-walking simulations at varying velocities are conducted in CoppeliaSim 4.5.1. The robot employed a control scheme as described in Sec3.2. The walking CoM height is maintained at 0.70m, and the gait period is set to 0.38s. The pre-contact point is selected as the operational point of swing foot, and the target trajectory was generated via a segmented Hermite Cubic Ppline. The desired CoM trajectory was generated by H-LIP orbit characterarion.

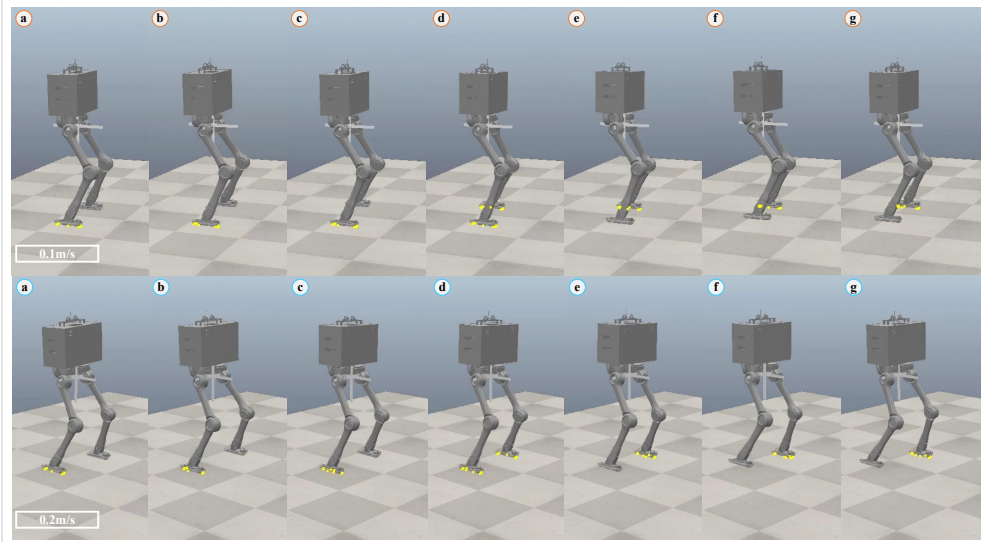


Fig. 4 Snapshots of the simulation at walking speeds of 0.1m/s and 0.2m/s.

The robot is required to perform sagittal plane walking at speeds of 0.1m/s and 0.2m/s, as in Fig4. The target joint-space trajectories were generated from Phased Inverse Kinematics(IK) which is solved by DRAKE, a robotic toolbox from MIT. The swing foot trajectory was treated as a hard position constraints, while the CoM trajectory, due to modeling errors, is not enforced as a constraint in the trajectory optimization. Instead, it was included as a cost term in the objective function. As discussed in Section2, we decoupled the swing foot and CoM trajectories into internal and external spaces, respectively. Finally, feedforward PD control with gravity compensation is engaged for tracking the target trajectories. The complete simulation videos are available on our GitHub. These results demonstrate that the proposed ESVC Foot and modeling approach enable stable locomotion of the robot.

4.2 Physical Evaluation

Three physical experiments are conducted on the TT II robot: marking time, straight walking, and lateral walking. Due to space limitations, the robot details can be found in our previous work[31].

4.2.1 Marking Time

Marking-time experiment are conducted on five different foot prototypes: flat foot, fine foot, ESVC1 Foot, ESVC2 Foot, and ESVC5 Foot. As shown in Fig5, all five foot types enabled stable marking-time walking. The lower subgraph of Fig5 presents the energy consumption over 30 seconds and one can be observed that the flat foot exhibits the highest cumulative energy consumption, while the Line Foot performs better than the flat foot. The ESVC foot consume less energy compared to both the

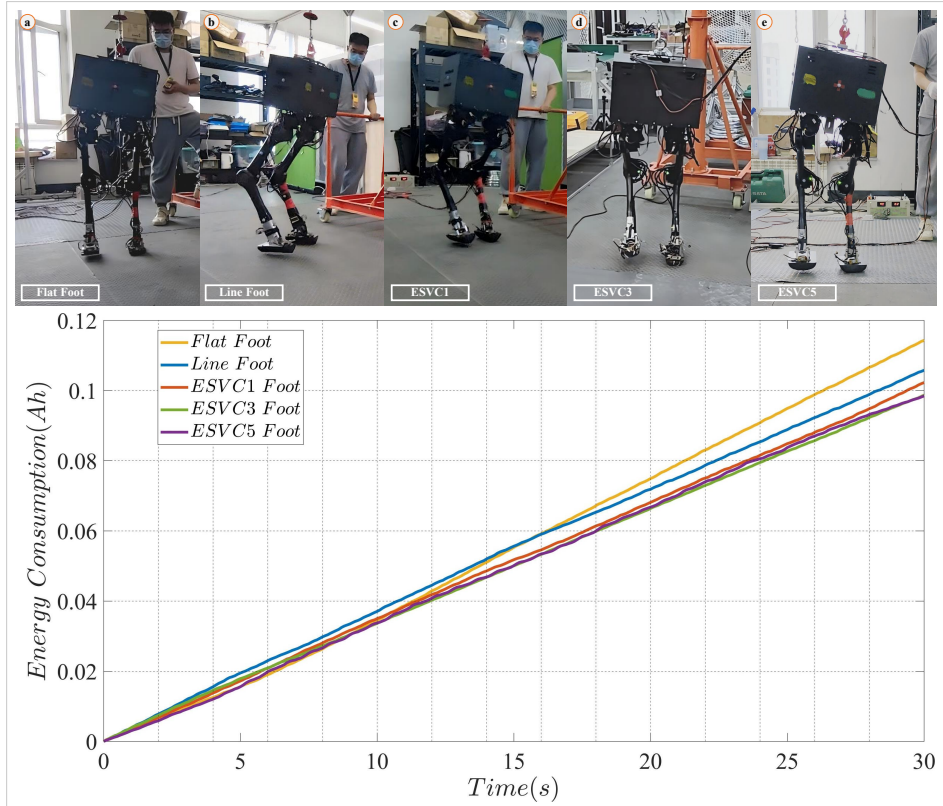


Fig. 5 a.Snapshots of marking time of robot TT II; b.The Total Energy Input;

flat and line Feet. Among the ESVC variants, the flatter ESVC5 shows the lowest energy consumption, whereas ESVC1 has the highest.

4.2.2 Straight Walking

We conducted sagittal plane straight walking experiments at speeds of 0.1m/s and 0.2m/s for all the foot types. Representative snapshots of the experiments are shown in the upper subgraph of Fig.6. The lower of Fig6 also presents the energy consumption over 30 seconds of walking. The energy efficiency trends are similar to the marking-time experiments: the ESVC5 Foot demonstrates the highest gait efficiency, while the flat foot shows the lowest.

4.2.3 Lateral Walking

Since the primary function of the ESVC Foot lies in the frontal plane, we also conducted physical experiments on lateral walking, as shown in the Fig.7. Due to the 5-DOF leg structure of the TT II robot lacking roll active freedom at the ankle, it is difficult to maintain frontal-plane balance with flat foot. Moreover, the results from marking-time and straight walking indicate that the energy consumption of the flat

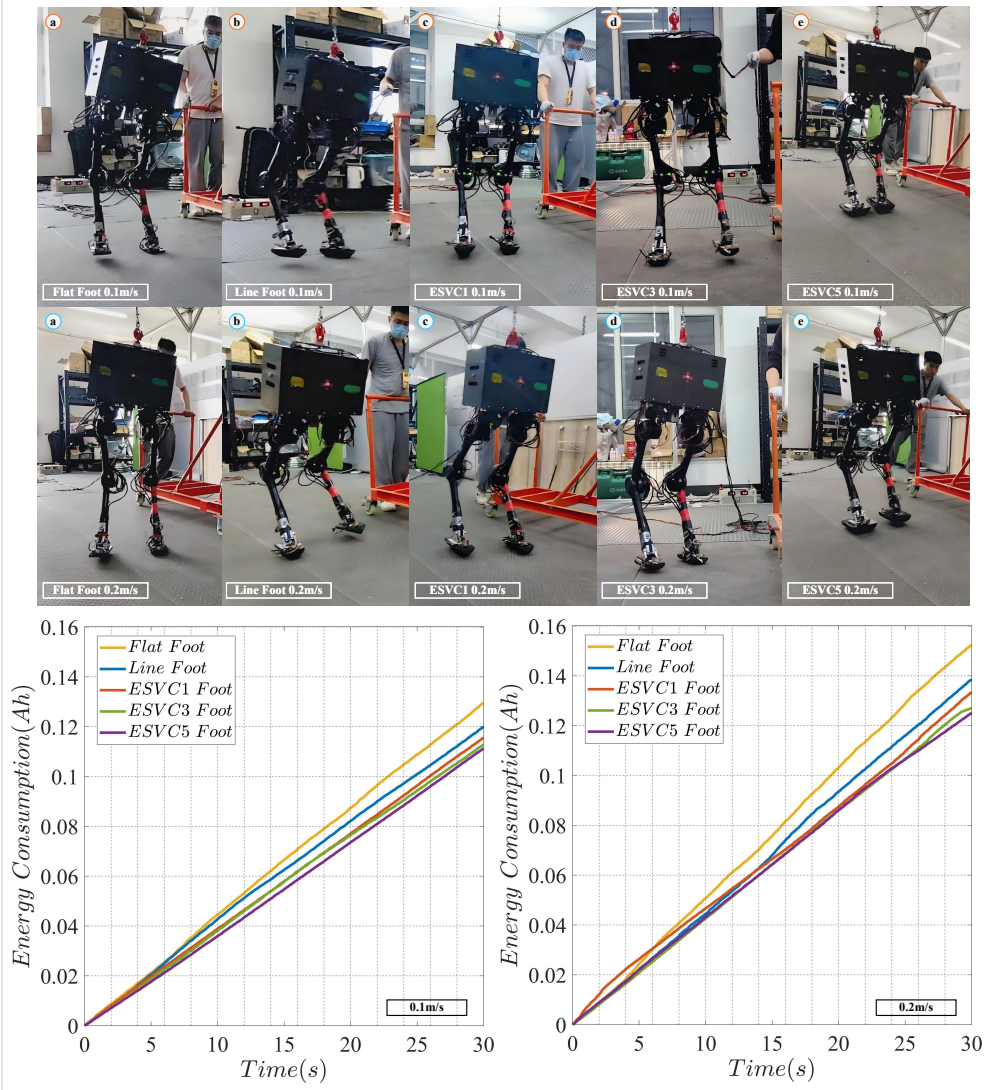


Fig. 6 a.Snapshots of straight walking of robot TT II; b.The Total Energy Input Of walking speeds of 0.1m/s; c.The Total Energy Input Of walking speeds of 0.2m/s;

foot is close to, and generally higher than the line foot. Therefore, we conduct the lateral walking without flat foot and selecting the line foot as the baseline for comparison with the ESVC foot. The cumulative energy consumption is shown in the lower subgraph of Fig 7. The result suggests that all ESVC foot types consumed less energy than the Line Foot. Among them, the ESVC5 Foot showed the lowest energy consumption, and the improvement in gait energy efficiency brought by the ESVC design becomes more pronounced at a speed of 0.2m/s.

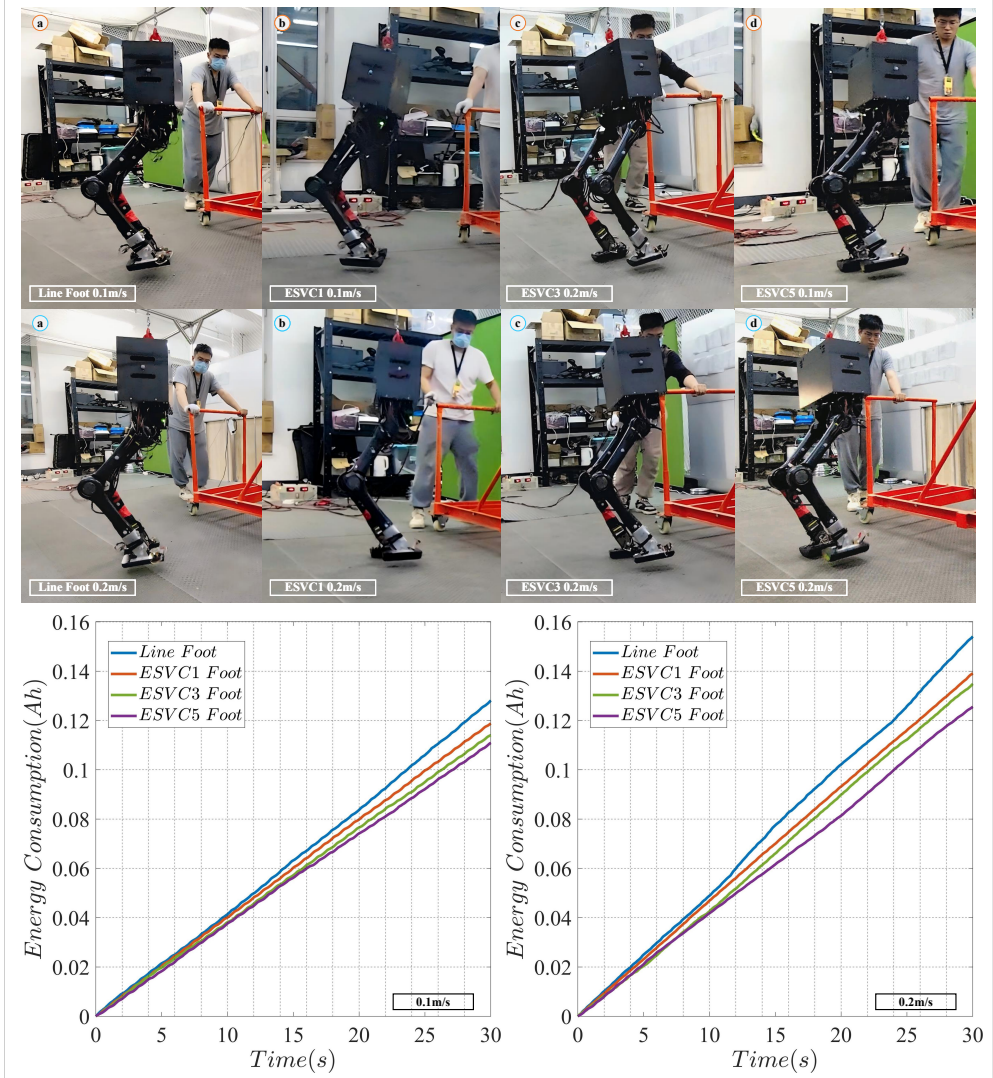


Fig. 7 a.Snapshots of lateral walking of robot TT II; b.The Total Energy Input Of walking speeds of 0.1m/s; c.The Total Energy Input Of walking speeds of 0.2m/s;

4.2.4 Analysis

The cumulative energy consumption observed across the three physical experiments confirms that the ESVC foot achieve better gait energy efficiency compared to the line foot and flat foot. To further investigate, we perform a quantitative analysis based on average power(P_{avg}).

$$P_{avg} = \frac{E_{total}}{Time} \quad (45)$$

The average gait power under different walking speeds and foot types is shown in Table2.

Table 2 Average Power Of Foot Prototypes at Different Walking Speed

	Maring Time	Sagittal Walking(0.1m/s)	Sagittal Walking(0.2m/s)	Lateral Walking(0.1m/s)	Lateral Walking(0.2m/s)
Flat	658.49	746.43	877.87	—	—
Line	609.45	691.14	798.55	738.07	887.62
ESVC1	589.21	665.74	768.87	685.35	801.45
ESVC3	568.60	650.08	731.89	656.85	776.74
ESVC5	567.24	640.90	721.25	639.01	723.19

From the table, we observe that during straight walking and marking-time walking, the flat foot exhibits the highest energy consumption approximately 8.04%(0.0m/s), 7.99% (0.1m/s), and 9.93% (0.2m/s) higher than the line foot, respectively. The ESVC prototypes offer more efficiency than the line foot. ESVC1 exhibits the closest performance that average power reductions of 3.32% (0.0m/s), 3.68% (0.1m/s), and 8.39% (0.2m/s). ESVC5 is the most efficient, achieving reductions about 6.93% (0.0m/s), 7.27% (0.1m/s), and 9.68% (0.2m/s). However, the improvement among the proposed types are relatively small, particularly between the ESVC1 and the line foot. The reason is that for marking-time and straight walking, the robot motion in the coronal plane is limited.

Among the ESVC variants, ESVC5 demonstrates the highest energy efficiency, while ESVC1 performs the worst. This is due to ESVC1 having the largest curvature, resulting in the smallest roll angle range during stance, making it functionally similar to the line foot when CoM fluctuation is small. Relatively, ESVC5 with the smallest curvature, allows the contact point to slide further along the rollover shape, which reduces impact energy dissipation. Additionally, this configuration shape is more closely resembles to the biological counterpart, thereby achieving the highest energy efficiency. During lateral walking, more significant improvements are observed. In the comparison at the speed of 0.1m/s, ESVC prototypes reduce average power consumption by 7.28%, 11.01%, and 13.32%, respectively, and at 0.2m/s, the reductions reach 6.80%, 12.49%, and 18.52%, respectively. This observation suggest that the

ESVC rollover shape with a relatively flatter midfoot tend to yield greater improvements in gait efficiency. In other words, the ESVC foot more closely approximates to a biological foot, resulting in superior energy performance.

5 Conclusion And Future Work

This paper presents a comprehensive study on the modeling and design of the ellipse-based segmented varying curvature (ESVC) foot. First, we derive the spatial transformations among three key frames which only relies on elementary function to construct the contact model. A nonlinear program based design approach is also provided. Then we conduct an accuracy analysis and an efficient piecewise compensation method is provided. Finally we integrated the ESVC foot into a model-based locomotion control framework. The physical experiments demonstrate that the proposed ESVC foot enables a stable walking and improves the gait energy efficiency, particularly with lateral velocity. The results suggest that the ESVC foot offers a practical and energy-efficient foot solution for legged-robot. However, several open questions still remain. First, we did not perform comparisons with other alternative methods. This is partly due to the limited research on ESVC foot, but more because of the lack of quantitative evaluation metrics. Second, a theoretical derivation of effectiveness and stability with model-based control are not provided. Third, the impact of ESVC modeling errors on system noise and body state estimation has not yet been investigated. These questions will be explored in our future research.

Declarations

- Ethics approval and consent to participate: Not applicable.
- Consent for publication: Not applicable.
- Data availability: Not applicable.
- Materials availability: Not applicable.
- Funding: This work was supported by the Major Research Plan of the National Natural Science Foundation of China (Grant No. 92048301).
- Conflict of interest/Competing interests: The authors declare that they have no known competing financial interests or personal relationships that could have appeared to influence the work reported in this paper.
- Code availability: Not applicable.
- Author contribution: Boyang Chen:Writing, Conceptualization of this study, Methodology, Software. Xizhe Zang:Conceptualization, Methodology, Resources. Chao Song:Conceptualization, Methodology, Software. Yue Zhang: Data curation, Writing. Ynaliu: Review&Editing. Jie Zhao: Resources.

References

- [1] J, L., S, F., J, T.: M-a3c a mean-asynchronous advantage actor-critic reinforcement learning method for real-time gait planning of biped robot. IEEE Access **10**, 76523–76536 (2022)

- [2] Ege M, K.S.: Energy minimization of new robotic-type above-knee prosthesis for higher battery lifetime. *Applied Sciences* **13**(6), 3868 (2023)
- [3] Mou H, L.J. Tang J: High dynamic bipedal robot with underactuated telescopic straight legs. *Mathematics* **12**(4), 600 (2024)
- [4] Curtze C, v.K.H.G. Hof A L: Comparative roll-over analysis of prosthetic feet. *Journal of biomechanics* **42**(11), 1746–1753 (2009)
- [5] Kwan M, H.M.: Optimal foot shape for a passive dynamic biped. *Journal of theoretical biology* **248**(2), 331–339 (2007)
- [6] Mei Q, X.L. Kim H K: Toward improved understanding of foot shape, foot posture, and foot biomechanics during running: A narrative reviews. *Frontiers in Physiology* **13**, 1062598 (2022)
- [7] Smyrli A, K.A. Ghiassi M: On the effect of semielliptical foot shape on the energetic efficiency of passive bipedal gait. *IEEE/RSJ International Conference on Intelligent Robots and Systems(IROS)* 6302-6307 (2019)
- [8] Ren L, R.L. Howard D: A generic analytical foot rollover model for predicting translational ankle kinematics in gait simulation studies. *Journal of biomechanics* **43**(2), 194–202 (2010)
- [9] Li, J., Tian Y, H.X.: Foot shape for passive dynamic kneed biped robot. *IEEE International Conference on Robotics and Biomimetics 2010* 1281–1286 (2016)
- [10] Piazza C, G.G.M. Della Santina C: Toward an adaptive foot for natural walking. *IEEE-RAS 16th International Conference on Humanoid Robots (Humanoids)* 1204-1210 (2016)
- [11] Mahmoodi P, F.M.I. Ransing R S: Modelling the effect of ‘heel to toe’roll-over contact on the walking dynamics of passive biped robots. *Applied Mathematical Modelling* **37**(12-13), 7352–7373 (2013)
- [12] Han L, Y.Z. Chen X: Trajectory-free dynamic locomotion using key trend states for biped robots with point feet. *Inf. Sci.* **66**(189201), 10–1007 (2023)
- [13] Liu Z, R.X. Gao J: Complex dynamics of the passive biped robot with flat feet: Gait bifurcation, intermittency and crisis. *Mechanism and Machine Theory*, (191), 105500 (2024)
- [14] García G, P.J. Griffin R: MPC-based locomotion control of bipedal robots with line-feet contact using centroidal dynamics. *IEEE-RAS 20th International Conference on Humanoid Robots (Humanoids)* 276-282 (2021)
- [15] Frizza I, C.A. Ayusawa K: Humanoids’feet: State-of-the-art and future directions. *International Journal of Humanoid Robotics* **19**(01), 2250001 (2022)

- [16] Gong Y, G.J.: Angular momentum about the contact point for control of bipedal locomotion: Validation in a lip-based controller. arXiv preprint (2020) [arXiv:2008.10763](https://arxiv.org/abs/2008.10763)
- [17] Pelit M M, T.R. Chang J: Bipedal walking based on improved spring loaded inverted pendulum model with swing leg (slip-sl). IEEE/ASME International Conference on Advanced Intelligent Mechatronics (AIM) 72-77 (2020)
- [18] Kuindersma S, F.M. Deits R: Optimization-based locomotion planning, estimation, and control design for the atlas humanoid robot. Autonomous robots **40**, 429–455 (2016)
- [19] Castillo G A, Z.W. Weng B: Robust feedback motion policy design using reinforcement learning on a 3d digit bipedal robot. IEEE/RSJ International Conference on Intelligent Robots and Systems (IROS) 5136-5143 (2021)
- [20] He Z, Z.J. Wu J: Cdm-mpc: An integrated dynamic planning and control framework for bipedal robots jumping. IEEE Robotics and Automation Letters (2024)
- [21] Gong Y, D.X. Hartley R: Feedback control of a cassie bipedal robot: Walking, standing, and riding a segway. American control conference (ACC) 4559-4566 (2019)
- [22] Adamczyk P G, K.A.D. Collins S H: The advantages of a rolling foot in human walking. Journal of experimental biology **209**(20), 3953–3963 (2006)
- [23] Kwan M, H.M.: Optimal foot shape for a passive dynamic biped. Journal of theoretical biology **248**(2), 331–339 (2007)
- [24] Yazdi-Mirmokhalesouni S D, Y.M.J. Sharbafi M A: Modeling, control and analysis of a curved feet compliant biped with hzd approach. Nonlinear Dynamics **91**, 459–473 (2018)
- [25] Silva C C D, G.L.C.S. Maximo M R O A: Energy efficient walking: combining height variation of the center of mass and curved feet. Journal of the Brazilian Society of Mechanical Sciences and Engineering **46**(6), 358 (2024)
- [26] Smyrli A, P.E.: Modeling, validation, and design investigation of a passive biped walker with knees and biomimetic feet. International Conference on Robotics and Automation (ICRA) 193-199 (2022)
- [27] Smyrli A, P.E.: A methodology for the incorporation of arbitrarily-shaped feet in passive bipedal walking dynamics. IEEE International Conference on Robotics and Automation (ICRA) 8719-8725 (2020)
- [28] Rodman C H, M.A.E.: Developing equations of motion for a planar biped walker

- with nonuniform foot shape. IFAC-PapersOnLine **54**(20), 455–462 (2021)
- [29] N., A.K.: Analytical determination of arc length of an elliptic curve. Mechanics of Solids **54**(7), 1115–1118 (2019)
- [30] Xiong X, A.A.: 3-d underactuated bipedal walking via h-lip based gait synthesis and stepping stabilization. IEEE Transactions on Robotics **38**(4), 2405–2425 (2022)
- [31] Chen B, Z.Y. Zang X: Symmetrical efficient gait planning based on constrained direct collocation. Micromachines **7**(4), 203 (2023)